Functional Analysis of the Rat I Sodium Channel in *Xenopus* Oocytes

Raymond D. Smith and Alan L. Goldin

Department of Microbiology and Molecular Genetics, University of California, Irvine, California 92697-4025

Voltage-gated sodium channels in the mammalian CNS initiate and propagate action potentials when excitatory inputs achieve threshold membrane depolarization. There are multiple sodium channel isoforms expressed in rat brain (types I, II, III, 6, and NaG). We have constructed a full-length cDNA clone encoding type I and compared the electrophysiological properties of type I (Rat1) and II (Rat2) channels in the absence and presence of the two accessory subunits β_1 and β_2. Injection into *Xenopus* oocytes of RNA encoding Rat1 resulted in functional sodium currents that were blocked by tetrodotoxin, with $K_{app} = 9.6$ nM. Rat1 sodium channels had a slower time course of fast inactivation than Rat2. Coexpression of β_1 accelerated inactivation of both Rat1 and Rat2, resulting in comparable inactivation kinetics. Rat1 recovered from fast inactivation more rapidly than Rat2, regardless of whether β_1 or β_2 was present. The voltage dependence of activation was similar for Rat1 and Rat2 without the β subunits, but it was more positive for Rat1 when β_1 and β_2 were coexpressed. The voltage dependence of inactivation was more positive for Rat1 than for Rat2, and coexpression with β_1 and β_2 accentuated that difference. Finally, sodium current amplitudes were reduced by 7–9% for both Rat1 and Rat2 channels when protein kinase A phosphorylation was induced. It has been suggested previously that Rat1 and Rat6 channels mediate transient and maintained sodium conductances, respectively, in Purkinje cells, and the electrophysiological properties of Rat1 currents are consistent with a role for this channel in mediating the rapidly inactivating, transient current.

Key words: sodium channel; cloning; expression; Xenopus *oocytes; brain; RT-PCR; protein kinase A; Purkinje cells*

Various sodium channel isoforms have been detected by molecular cloning, biochemical purification, and electrophysiological recording (for review, see Goldin, 1995). Multiple isoforms have been identified in the rat CNS, including types I (Rat1) (Noda et al., 1986a), II (Rat2) (Noda et al., 1986a) and a splice variant termed Rat2A (Auld et al., 1988), III (Rat3) (Kayano et al., 1988; Joho et al., 1990), 6 (Rat6) (Schaller et al., 1995) and the species variant Scn8a (Burgess et al., 1995), and a partial cDNA sequence for NaG (Gautron et al., 1992). In addition to the pore-forming α subunit of the sodium channel, there are two accessory subunits termed β_1 and β_2 (Hartshorne and Catterall, 1984). The β_1 subunit modulates channel function by accelerating the kinetics of inactivation and shifting its voltage dependence in the hyperpolarizing direction (Isom et al., 1992). The β_2 subunit is covalently bound to the α subunit, and it accelerates inactivation slightly (Isom et al., 1995).

The sodium channel isoforms in the CNS are present at different times during development and in different locations. Rat1 becomes detectable shortly after birth and increases until adulthood, Rat2 becomes detectable during embryonic development and reaches maximal levels during adulthood, Rat3 peaks at birth and becomes undetectable by adulthood (Beckh et al., 1989), and Rat6 peaks during late embryonic and early postnatal periods (Felts et al., 1997) but is also present at high levels during adulthood (Schaller et al., 1995). Levels of Rat2 are highest in the rostral regions of the CNS, Rat1 is the predominant channel in the caudal regions and the spinal cord (Gordon et al., 1987; Beckh et al., 1989), and there is no rostral–caudal gradient of Rat6 mRNA (Schaller et al., 1995). In the cerebellum, Rat1 is detectable in Purkinje cells but not in granule cells, Rat2 is expressed in both Purkinje (Black et al., 1994) and granule cells (Furuyama et al., 1993), and Rat6 is expressed predominantly in granule cells (Schaller et al., 1995). Rat1 is localized in the soma of neurons in various CNS regions, including the hippocampus, cerebellum, and spinal cord, whereas Rat2 is axonal in distribution (Westenbroek et al., 1989). Because there are multiple α sodium channel isoforms in the mature brain, it is conceivable that each has a distinct role in determining electrical excitability. For example, Rat1 and Rat6 channels have been predicted to mediate transient and maintained sodium conductances, respectively, in Purkinje cells (Vega-Saenz de Miera et al., 1997).

By examining the functional properties of the different sodium channel isoforms, it should be possible to gain a better understanding of how each isoform affects electrical excitability. The properties of the Rat2 (Auld et al., 1988) and Rat3 (Joho et al., 1990) sodium channels have been extensively characterized, but neither the Rat1 nor Rat6 channels have been expressed in an exogenous system. Attempts to characterize the properties of the original Rat1 clone in *Xenopus* oocytes were unsuccessful (Noda et al., 1986a), and that clone has not been available for study. We therefore constructed a full-length clone encoding Rat1 and compared the functional properties of Rat1 and Rat2 channels in the absence and presence of β_1 and β_2 subunits.

MATERIALS AND METHODS

Isolation of rat brain RNA. Total rat brain RNA was isolated from 15 to 18-d-old rats by a modified lithium chloride/urea procedure (Dierks et al.,

Received Aug. 20, 1997; revised Oct. 6, 1997; accepted Nov. 6, 1997.

This research was supported by National Institutes of Health Grant NS 26729 to A.L.G. A.L.G. is an Established Investigator of the American Heart Association. We thank Drs. Linda Hall, Marianne Smith, Ted Shih, and Michael Pugsley for helpful discussions during the course of this work, and Dr. Linda Hall and Mike Wishingrad for the sequencing. We acknowledge Esther Yu and Mimi Reyes for excellent technical assistance.

Correspondence should be addressed to Dr. Alan L. Goldin, Department of Microbiology and Molecular Genetics, University of California, Irvine, CA 92697-4025.

1981). RNA was suspended in sterile, RNase-free water at a concentration of 1 mg/ml and stored at −75°C.

Reverse transcription and PCR. The Rat1 coding region was amplified from total rat brain RNA by reverse transcription followed by PCR (RT-PCR) in two fragments, with the middle boundary defined by the unique SphI site in the coding region. Primers for reverse transcriptase and PCR were designed based on the published sequence (Noda et al., 1986b). The four primers used were (A) 5′ end primer: 5′-GGCCATAT-(GCGGCCGC)ATCAGGAATCTCACATGAAG-3′; (B) primer upstream of SphI (5′): 5′-CTGGTGCTGGCCATCATCG-3′; (C) primer downstream of SphI (3′): 5′-GCAGTCAGTGGCAATTTTGC-3′; and (D) 3′ end primer: 5′-GGCCATAT(GCGGCCGC)AGTCCTTTGA-CTTCACAGG-3′. Each of the outer 5′ and 3′ primers contains a four-base G–C clamp and an extra four nucleotides to promote efficient cutting at the NotI sites (indicated in parentheses).

Total brain RNA (2 μg) was heat-denatured at 65°C for 5 min, followed by rapid cooling on ice. RT was performed with 0.5 mM deoxynucleotide triphosphates, 10 mM dithiothreitol, 100 pmol of oligonucleotide primers (C and D), 40 U RNasin (Promega, Madison, WI), and 500 U M-MLV reverse transcriptase (Life Technologies, Gaithersburg, MD) in a total volume of 50 μl. Reactions were incubated at room temperature for 5 min and then at 37°C for 2 hr. Reaction products were purified by phenol/chloroform extraction and ethanol precipitation and were resuspended in 10 μl of distilled water.

The two RT products were amplified using the primer pairs A–C (amino terminal portion of Rat1) and B–D (carboxy portion of Rat1). The RT product was combined with 2.5 mM $MgCl_2$, 200 μmol deoxynucleotide triphosphates, 0.2 μM of each primer, and 2.5 U LA Taq Polymerase (PanVera, Madison, WI). Thermal cycle parameters for A–C primer amplification were one cycle consisting of denaturation at 95°C for 4 min, annealing at 50°C for 3 min, and polymerase extension at 72°C for 6 min, followed by 30 cycles consisting of denaturation at 95°C for 30 sec, annealing at 50°C for 1 min, and polymerase extension at 72°C for 6 min. Parameters for B–D amplification were the same except that annealing steps were at 55°C. These conditions resulted in two PCR fragments of size 3429 and 2851 bp for primer pairs B–D and A–C, respectively. These fragments were extracted with phenol/chloroform, precipitated with ethanol, and resuspended in distilled water before digestion with the appropriate restriction enzymes.

Construction of full-length Rat1 cDNA. The full-length cDNA for Rat1 was constructed by making a series of Rat1–Rat2 chimeras and then combining Rat1 sequences. Chimeras were constructed using AatII and SphI restriction sites that are common to both channels. The B–D PCR product (carboxy end of Rat1) was cloned into the corresponding region of Rat2 using SphI and NotI restriction sites to generate a chimeric Rat2–1 channel (written Rat2211, with each number corresponding to approximately one domain of the channel). This chimera expressed sodium current in oocytes (data not shown).

A Rat1–2 chimera (Rat1122) was constructed by ligation of the Rat1 amino terminal PCR product A–C (NotI–SphI) with the complementary Rat2 SphI–NotI fragment into the NotI site of pLCT1, a modified version of pBSTA (Goldin, 1991) that contains the gene for tetracycline resistance and an origin of replication from the plasmid pACYC184. An isolate was obtained that contained Rat1 sequence positioned downstream from the T3 promoter; however, RNA transcribed by T3 RNA polymerase did not express sodium current in oocytes. To transfer additional Rat1 sequence into Rat2211, the AatII–SphI region from Rat1122 (domain 2) was incorporated to yield a Rat2111 chimera. This chimera did express sodium current in oocytes.

We reasoned that the lack of expression by the Rat1122 construct was most likely attributable to three extra ATG start codons that followed the T3 promoter but were upstream and in a different reading frame than the authentic start codon. Therefore, the 5′ region was modified by a secondary round of PCR to exclude the three extra start codons and to attach an XhoI site at the 5′ end for subsequent ligation into the XhoI site in Rat2. The modification was accomplished using a new 5′ primer [GCGCGC(CTCGAG)TGACAAGATGGAGCAAAC (XhoI site in parentheses)] and a new primer downstream from the AatII restriction site CACACTGAGACAGAACACGG. The second round of PCR was performed using 2 ng of Rat1122 plasmid DNA, 20 μM deoxynucleotide triphosphates, 1 μM each primer, and 2.5 U Pfu DNA polymerase (Stratagene, La Jolla, CA). Thermal cycling parameters were as described for the initial RT-PCR, except that the annealing temperature was 57°C. The secondary PCR product (801 bp) was cut with XhoI and AatII and ligated into the corresponding sites in Rat2111 to construct the full-length Rat1 sequence (Rat1111). Expression of sodium current was observed in oocytes after injection of RNA transcribed from this clone.

The sequence of the entire coding region was determined using the dideoxy chain termination method and the Taq dye terminator cycle sequencing kit with an Applied Biosystems sequencer Model 373 Stretch (Applied Biosystems). To increase the level of expression in oocytes, the Rat1 coding region was inserted into the BgIII site of pLCT1, which resulted in the 5′ and 3′ noncoding regions from the *Xenopus* β-globin gene being positioned on either side of the Rat1 coding region and a poly-A tail at the 3′ end of the insert. The Rat1 coding region was inserted into pLCT1 by cutting it with XhoI and NotI, followed by generation of blunt ends with Klenow DNA polymerase, attachment of BgIII linkers, and ligation into the BgIII site of pLCT1.

Complementary DNA clones encoding the β_1 subunit (Isom et al., 1992) and β_2 subunit (Isom et al., 1995) were isolated from total rat brain RNA by RT-PCR, using published sequence information to design the following primers: β_1(5′)-TCGAGATCTATGGGGACGCTGCT; β_1-(3′)GCCAGATCTATTCAGCCACCTGG; β_2(5′)-GCATCGATGG-CCTGAAAATGCACAGGGATGC; and β_2(3′)-GCATCGATGGATC-CGGACACAGGAAGGGGCTTC. RT and PCR conditions were similar to those used for Rat1, except that annealing temperatures were adjusted to 5°C below the melting temperature of each primer pair.

Expression and electrophysiology. RNA transcripts were synthesized from NotI linearized DNA templates using a T7 RNA polymerase Message Machine transcription kit (Ambion, Austin, TX). The yield of RNA was estimated by glyoxal gel analysis. Stage V oocytes were removed from adult female *Xenopus laevis* frogs and prepared as described previously (Goldin, 1991), and incubated in ND-96 media, which consists of (in mM) 96 NaCl, 2 KCl, 1.8 $CaCl_2$, 1 $MgCl_2$, and 5 HEPES, pH 7.5, supplemented with 0.1 mg/ml gentamicin, 0.55 mg/ml pyruvate, and 0.5 mM theophylline. Rat2 sodium channel RNA was injected at 100 pg/oocyte, and Rat1 RNA was injected at 50 ng/oocyte. The oocytes were incubated for 40 hr at 20°C in ND-96.

Sodium currents were recorded using the cut-open oocyte technique (Taglialatela et al., 1992) with the CA-1 high performance oocyte voltage clamp (Dagan, Minneapolis, MN) and Digidata 1200A interface (Axon Instruments, Foster City, CA) and pCLAMP 6.0.3 software (Axon Instruments), as described previously (Kontis et al., 1997). Temperature was maintained at 20°C using an HCC-100A temperature controller (Dagan). The intracellular solution consisted of (in mM) 88 K_2SO_4, 10 EGTA, 10 HEPES, 10 Na_2SO_4, pH 7.5, and the extracellular solution consisted of (in mM) 120 sodium MES, 10 HEPES, and 1.8 Ca–Cs, pH 7.4. Capacitive transients and leak currents were corrected by P/4 subtraction. Sodium current amplitudes were between 1 and 5 μA.

For analysis of recovery from inactivation and modulation by protein kinase A (PKA), a two-electrode voltage clamp was used at room temperature as described previously (Patton and Goldin, 1991). Although this voltage clamp does not provide the fast time resolution of the cut-open oocyte clamp, the oocytes are more stable over long periods of time, which was essential for analyzing these two channel properties. Capacitive and leak currents were eliminated from the recovery from inactivation records by subtraction of comparable records obtained in the presence of 400 nM tetrodotoxin, and from the PKA modulation records by P/4 subtraction. The bath solution consisted of ND-96. Oocytes were clamped at −100 mV for 5–10 min before recording to allow for recovery from slow inactivation. After steady-state current levels were established for 10 min, PKA was induced by perfusing oocytes with a mixture consisting of 25 μM forskolin, 10 μM chlorophenylthio-cAMP (cpt-cAMP), 10 μM dibutyryl-cAMP (db-cAMP), and 10 μM 3-isobutyl-1-methylxanthine (IBMX) for 10 min. We have shown previously that this mixture reduces Rat2 sodium currents by activation of PKA (Smith and Goldin, 1997). The rate of bath perfusion was carefully adjusted to 0.3 ml/min to minimize fluctuations in current amplitude resulting from changes in flow rate. Sodium current amplitudes were measured every 60 seconds during depolarizations to −10 mV from a holding potential of −100 mV.

Data analysis. Analysis was performed using pCLAMP 6.0.3 software (Axon Instruments), Excel 7.0 (Microsoft, Redmond, WA), and Sigmaplot 4.0 (Jandel, San Rafael, CA). Inactivation time constants were determined using the Chebyshev method to fit current traces with a single exponential equation: $I = A_{slow} \cdot \exp[-(t - K)/\tau_{slow}] + C$, or a double exponential equation: $I = A_{fast} \cdot \exp[-(t - K)/\tau_{fast}] + A_{slow} \cdot \exp[-(t - K)/\tau_{slow}] + C$, where I is the current, A_{fast} and A_{slow} represent the percentage of channels inactivating with time constants τ_{fast} and τ_{slow}, K is the time shift, and C is the steady-state asymptote. The time shift was

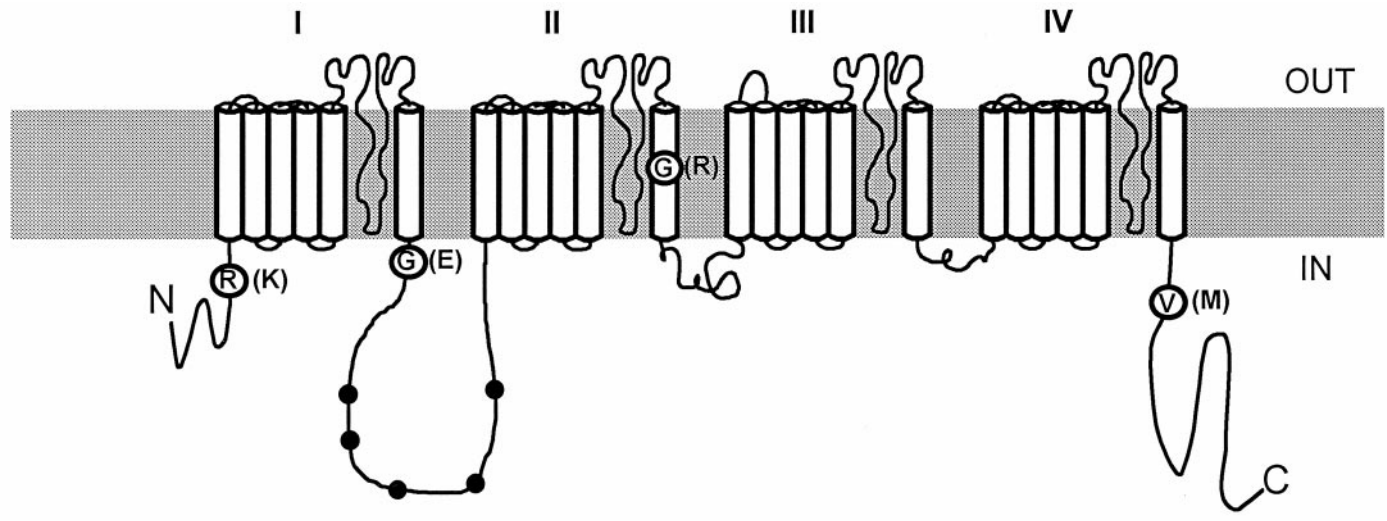

Figure 1. Diagram of the Rat1 sodium channel. The predicted transmembrane topology of the voltage-gated sodium channel consists of four homologous domains (I–IV), each composed of eight transmembrane segments. The linkers connecting the four domains and the amino and C termini are on the inside of the membrane. The four amino acids that differ between the cDNA clone described in this paper (*circled*) and the cDNA clone originally isolated by Noda et al. (1986a) (*parentheses*) are indicated. The five consensus PKA sites in the I–II linker are depicted by *solid circles*.

manually selected by fitting the traces at the time when the currents were just starting to decrease exponentially. Recovery data were fit using a double or triple exponential equation of the form $I = 1 - [A_1 \cdot \exp(-t/\tau_1) + A_2 \cdot \exp(-t/\tau_2)]$ and $I = 1 - [A_1 \cdot \exp(-t/\tau_1) + A_2 \cdot \exp(-t/\tau_2) + A_3 \cdot (-t/\tau_3)]$, where A_1, A_2, and A_3 are the relative proportions of current recovering with time constants τ_1, τ_2, and τ_3, and t is the recovery interval.

Conductance values were calculated using the formula $G = I/(V - V_r)$, where G is conductance, I is current amplitude, V is the depolarized membrane potential, and V_r is the reversal potential. Reversal potentials were individually estimated for each data set by fitting the *I–V* data with the equation $I = [1 + \exp(-0.03937 \cdot z \cdot (V - V_{1/2}))]^{-1} \cdot g \cdot (V - V_r)$, where z is the apparent gating charge, g is a factor related to the number of channels contributing to the macroscopic current, V is equal to the voltage potential of the pulse, and $V_{1/2}$ is the half-maximal voltage. Conductance values were fit with a two-state Boltzmann equation, $G = 1/(1 + \exp[-0.03937 \cdot z \cdot (V - V_{1/2})])$, with z equal to the apparent gating charge, V equal to the pulse potential, and $V_{1/2}$ equal to the voltage required for half-maximal activation. The voltage dependence of fast inactivation data was fit with a two-state Boltzmann equation, $I = 1/(1 + \exp[(V - V_{1/2})/a])$, with I equal to the current amplitude measured during the test depolarization, V equal to the inactivating depolarization potential, a equal to the slope factor, and $V_{1/2}$ equal to the voltage depolarization required for half-maximal inactivation. For analysis of current after PKA induction, there was drift in the peak current amplitude in some cases, even after allowing for recovery from slow inactivation. In those cases, the peak current measurements were adjusted by subtracting a linear relationship that was fit to data acquired during the first 10 min before PKA stimulation.

RESULTS

Construction of a full-length cDNA clone encoding the Rat1 sodium channel

The type I rat brain sodium channel sequence (Rat1) was amplified by RT-PCR from total rat brain RNA using primers based on the previously published sequence (Noda et al., 1986a). The continuous, full-length cDNA containing the coding region was sequenced to determine the predicted amino acid sequence. The sequence of this clone is similar to that of the previously published Rat1 sequence (Noda et al., 1986a). The two sequences differ at only 11 nucleotide positions. Most of these differences are silent, so that there are only four amino acid differences, which are represented by the circled residues in Figure 1. The amino acid indicated within each circle is the residue present in the clone that we have constructed, and the amino acid indicated in parentheses is present in the clone isolated by Noda et al. (1986a). Three of the differences are located in putative cytoplasmic regions of the channel (R97K, G427E, and V1823M), and two of these (R97K and V1823M) are conservative changes. The final difference (G979R) is a nonconservative change in the S6 transmembrane region of domain II.

Functional expression of Rat1 sodium channels and modulation by β_1 and β_2

RNA encoding the Rat1 sodium channel was transcribed *in vitro* and injected into *Xenopus* oocytes, which resulted in significant levels of sodium current. The Rat1 current was sensitive to tetrodotoxin, with a $K_{app} = 9.6 \pm 3.2$ nM, similar to the value obtained for Rat2 currents in this study (8.8 ± 4.0 nM). Sodium currents were recorded using a cut-open oocyte voltage clamp, and the properties of Rat1 were compared with those of Rat2 (Fig. 2). Both channel isoforms were tested by injection of RNA encoding the α subunit alone, $\alpha + \beta_1$ subunits, $\alpha + \beta_2$ subunits, and $\alpha + \beta_1 + \beta_2$ subunits. Sodium currents were elicited by depolarizations ranging from −65 to +25 mV in 10 mV increments from a holding potential of −100 mV. To obtain comparable levels of current for the two channels, a 500-fold greater amount of Rat1 RNA was injected. The properties of both Rat1 and Rat2 were modulated by β_1, most notably resulting in an accelerated time course of fast inactivation (Fig. 2*B*). The β_2 subunit resulted in a slight acceleration of inactivation that was more pronounced for Rat1 (Fig. 2*C*). The combination of β_1 and β_2 resulted in kinetics of inactivation that were similar to those observed when just β_1 was added to either α subunit (Fig. 2*D*). The effects of β_1 and β_2 on Rat2 are consistent with previous studies (Isom et al., 1992, 1995; Patton et al., 1994).

Rat1 sodium channels inactivate more slowly than Rat2 channels

In the absence of β_1 and β_2, the Rat1 currents demonstrated a slower time course of fast inactivation than did the Rat2 currents (Fig. 2*A*). To quantify the differences, the time constants for inactivation were determined by fitting the current traces with

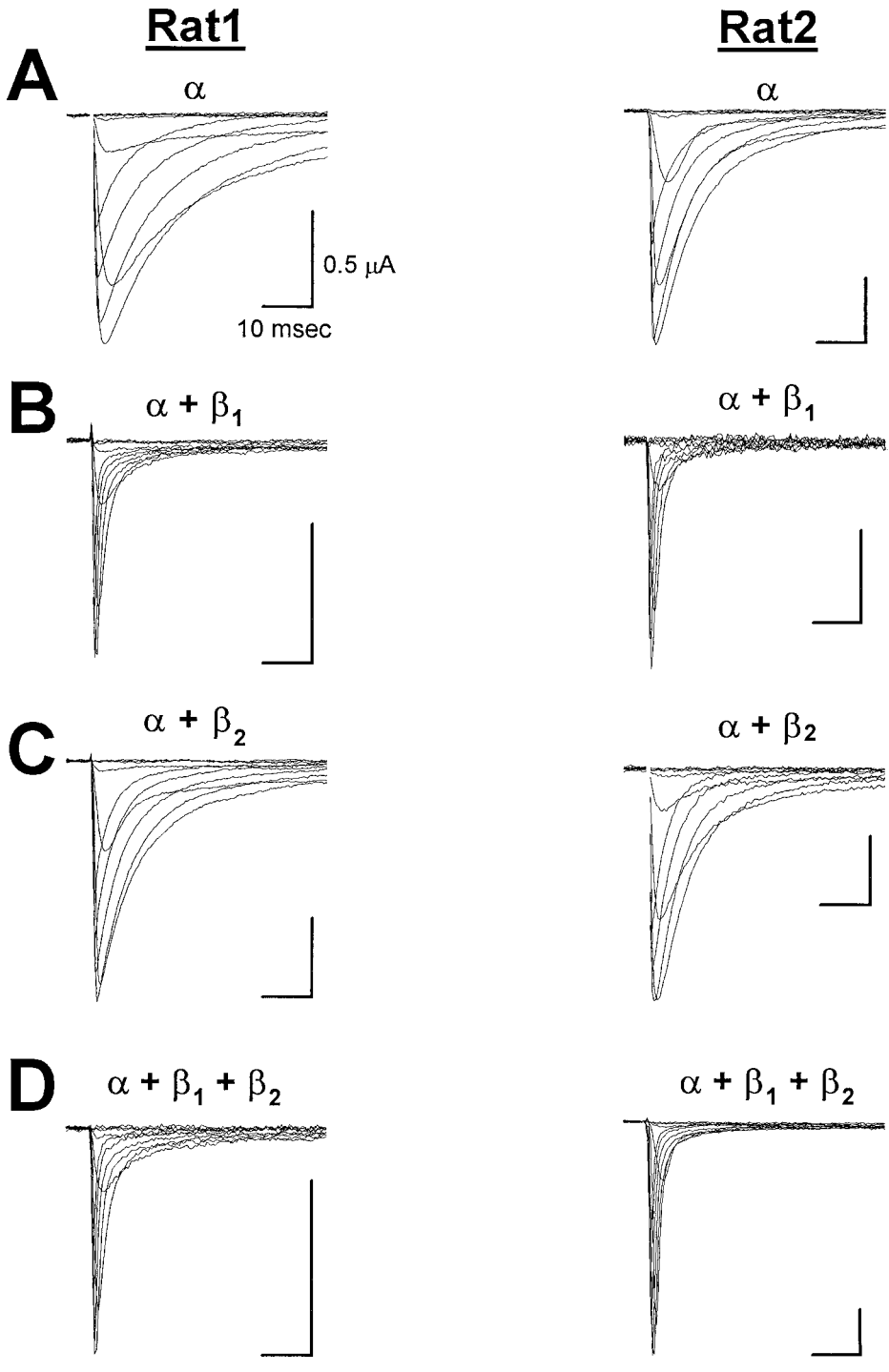

Figure 2. Representative Rat1 and Rat2 sodium channel currents. Rat1 and Rat2 sodium currents are compared for (*A*) α subunits alone, (*B*) $\alpha + \beta_1$ subunits, (*C*) $\alpha + \beta_2$ subunits, and (*D*) $\alpha + \beta_1 + \beta_2$ subunits. Rat1 and Rat2 sodium channels were expressed in *Xenopus* oocytes, and currents were recorded using a cut-open oocyte voltage clamp at 20°C as described in Materials and Methods. Currents were elicited by membrane depolarizations ranging from −65 to +25 mV in 10 mV increments from a holding potential of −100 mV. Calibration: 10 msec, 0.5 μA.

single and double exponential equations, as described in Materials and Methods (Fig. 3*A*). For depolarizations between −30 and 0 mV, current traces were fit with a single exponential equation, resulting in one time constant of inactivation (τ_{slow}, *squares*). For depolarizations between +10 mV and +50 mV, current traces were best fit with a double exponential equation, resulting in two time constants (τ_{fast}, *circles*, and τ_{slow}, *squares*). The time constants for both components of inactivation were significantly greater for Rat1 (*filled symbols*) than for Rat2 (*open symbols*). The fraction of current represented by τ_{fast} is indicated in the bottom panel of Figure 3. The fraction represented by τ_{fast} is 0 between −30 mV and 0 mV, because those traces were fit with a single exponential equation representing the slow time constant. Between +10 mV and +50 mV, the fast component of inactivation became increasingly prominent, as indicated by the fraction of current that was fit with τ_{fast}. At depolarizations equal to or greater than +20 mV, both channel isoforms demonstrated approximately equal fractions of the fast and slow components.

When Rat1 and Rat2 were coexpressed with the β_1 subunit, sodium current traces were best fit with two exponential equations over the entire range of depolarizations (Fig. 3*B*). The principal effect of β_1 for both channels was to accelerate the fast component

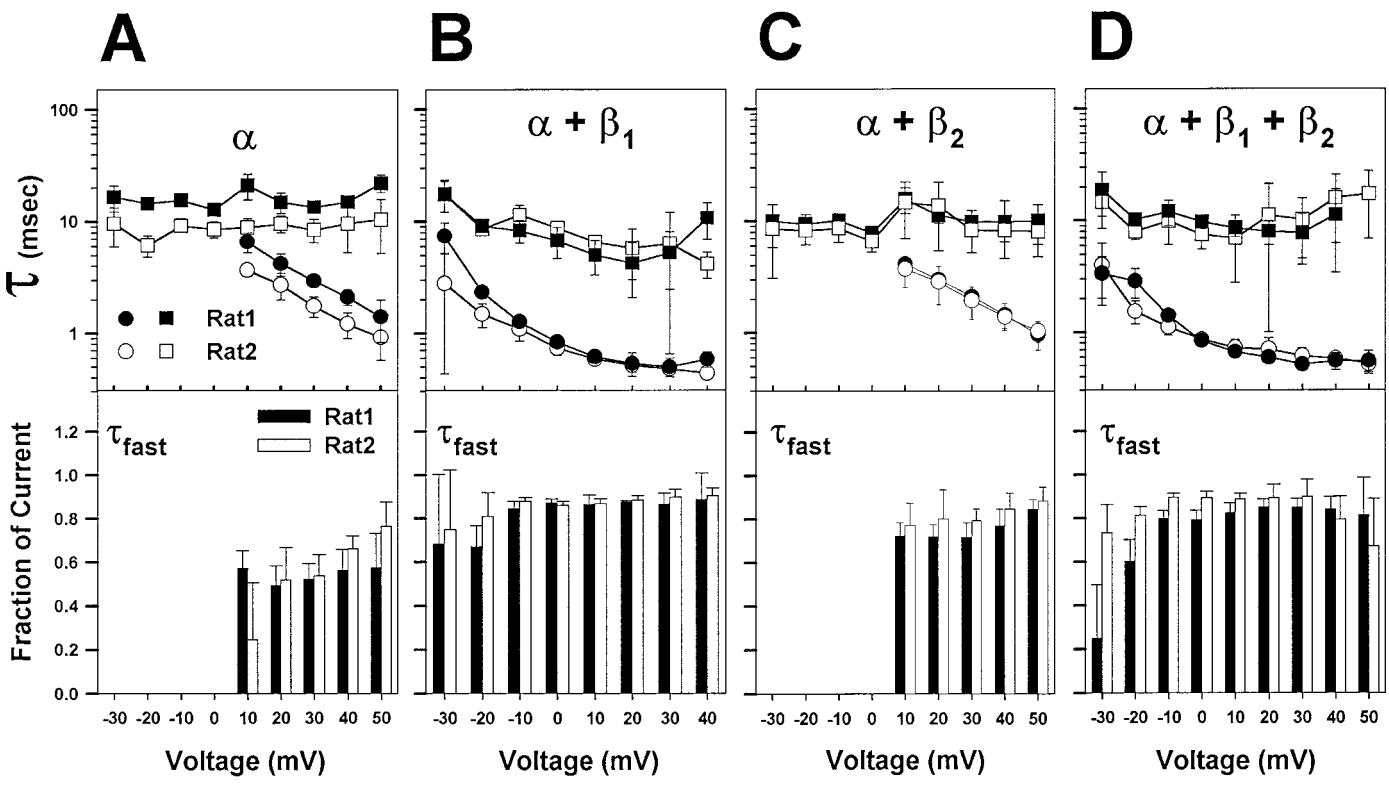

Figure 3. Time constants for fast inactivation of Rat1 and Rat2 sodium channels. Currents were recorded from oocytes expressing Rat1 or Rat2 sodium channels as described in the legend to Figure 2. The kinetics of inactivation were fit with single or double exponential equations as described in Materials and Methods, and the time constants representing the fast and slow components are shown on a logarithmic scale in the *top panels* for (*A*) α subunits alone, (*B*) α + β_1 subunits, (*C*) α + β_2 subunits, and (*D*) α + β_1 + β_2 subunits. The fast component (τ_{fast}) is represented by *circles*, and the slow component (τ_{slow}) is represented by *squares*. *Solid symbols* indicate Rat1 (●, ■), and *open symbols* indicate Rat2 (○, □). The fraction of current inactivating with τ_{fast} is shown in the *bottom panels*. *Solid bars* indicate Rat1, and *open bars* indicate Rat2. In all cases, the fraction of τ_{fast} plus the fraction of τ_{slow} equals 1. Values represent averages, and error bars indicate SDs. Sample sizes were Rat1 α (7), Rat2 α (9), Rat1 α + β_1 (5), Rat2 α + β_1 (7), Rat1 α + β_2 (6), Rat2 α + β_2 (5), Rat1 α + β_1 + β_2 (7), and Rat2 α + β_1 + β_2 (6).

of inactivation, as has been shown previously to be the case for Rat2 (Isom et al., 1992; Patton et al., 1994). The β_1 subunit had a somewhat greater effect on Rat1 currents, so that τ_{fast} values for both channel isoforms were comparable in the presence of β_1. In addition, β_1 caused the fast component to predominate for both Rat1 and Rat2 throughout the entire range of depolarizations tested (Fig. 3*B*, *bottom panel*). The effect of β_1 on τ_{slow} was to cause a considerable reduction for Rat1 and a slight reduction for Rat2, so that the time constants in the presence of β_1 were comparable. Therefore, β_1 caused both channel isoforms to be functionally equivalent with respect to τ_{fast} and τ_{slow}.

When Rat1 and Rat2 were coexpressed with the β_2 subunit, the kinetics were best fit with a single exponential (τ_{slow}) between −30 and 0 mV, and two exponentials between +10 and +50 mV (Fig. 3*C*). These results were similar to those observed when the α subunits were expressed alone, with one notable difference. The kinetics of inactivation for the Rat1 channel were accelerated significantly, and there was only a minimal effect on the Rat2 channel. Therefore, the kinetics of inactivation were comparable for Rat1 and Rat2 in the presence of the β_2 subunit.

Coexpression of β_1 and β_2 produced a modest increase in τ_{slow} compared with β_1 alone over a range of depolarizations for Rat1 (Fig. 3*D*). In addition, a smaller fraction of Rat1 channels inactivated with the fast component at more negative depolarizations. Most notably, the fraction of τ_{fast} at −30 mV was only 25%, but that fraction increased to 80% by −10 mV (Fig. 3*D*, *bottom panel*). The combination of β_1 and β_2 resulted in inactivation kinetics of Rat2 that were comparable to those observed in the presence of β_1 alone.

Recovery from inactivation is faster for Rat1 compared with Rat2 sodium channels

Because Rat1 differed from Rat2 with respect to the kinetics of entry into the inactivated state, it was likely that the two channels would also differ with respect to the kinetics of recovery from inactivation. We therefore examined the kinetics of recovery from inactivation of Rat1 and Rat2 sodium channels. A two-pulse protocol was used to measure recovery over a time interval of 1–3000 msec, as described in the legend to Figure 4. The kinetics of recovery for Rat1 and Rat2 without β subunits are shown on a log scale in Figure 4*A*. Recovery is a multicomponent process for both channels, as can be seen by the multiple slopes of the curves. The kinetics were fit with a triple exponential equation as described in Materials and Methods, and the values for the time constants are shown in Table 1. The time constants for all three components of recovery are smaller for Rat1 than for Rat2, although this is somewhat offset by the fact that a greater percentage of Rat1 current recovered with the slowest time constant (τ_3). In general, however, Rat1 recovered from inactivation more rapidly than Rat2.

When the β_1 subunit was coexpressed with the α subunits, recovery from inactivation was faster for both Rat1 and Rat2, with Rat1 recovering more quickly than Rat2 at short recovery times

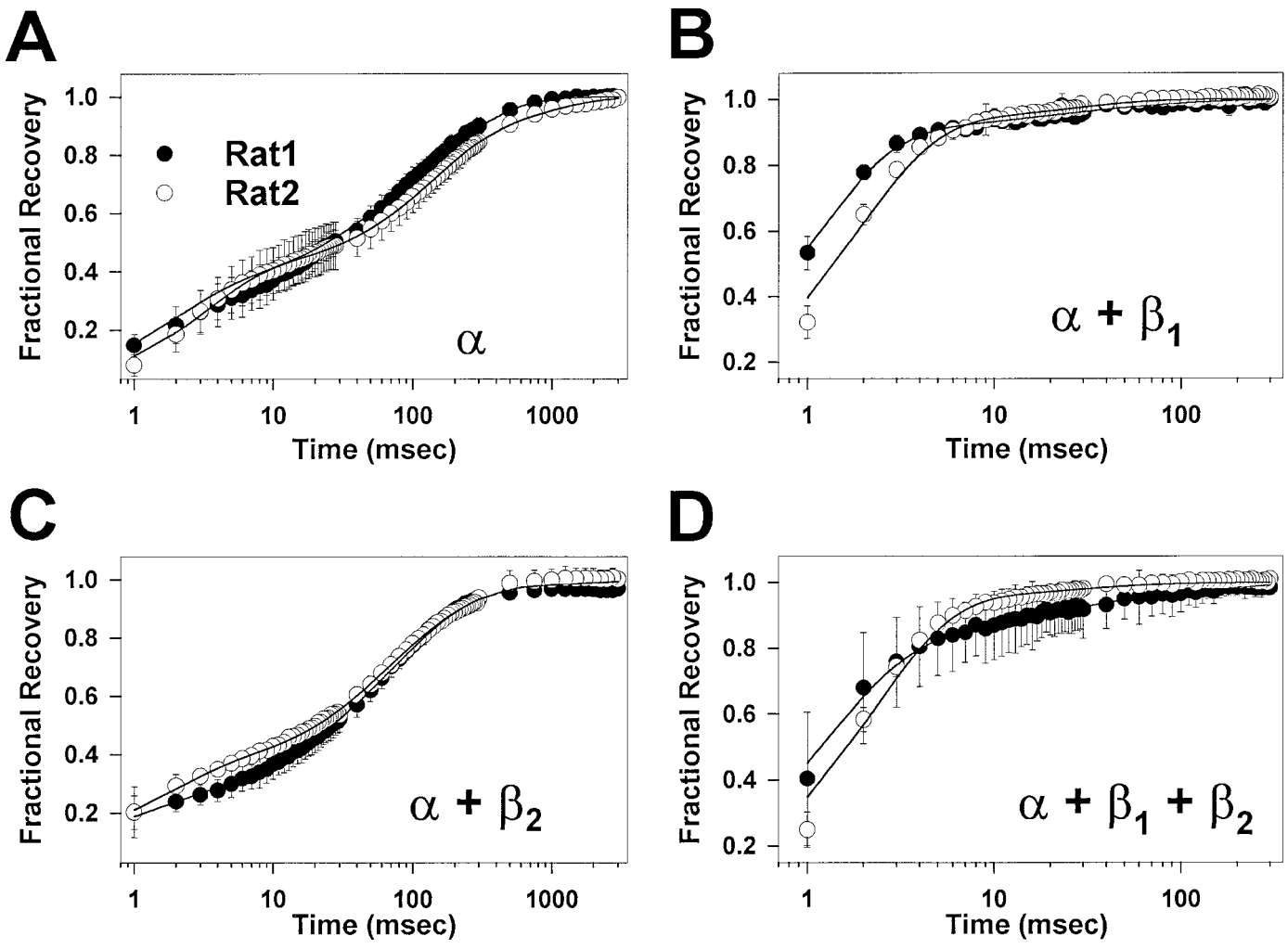

Figure 4. Recovery from fast inactivation of Rat1 and Rat2 sodium currents. Recovery from inactivation was measured using a two-pulse protocol consisting of an initial conditioning pulse to −10 mV for 50 msec (which inactivated >95% of the channels), a variable recovery interval, and a test pulse to −10 mV to measure the amount of current that had recovered. Fractional recovery was calculated by dividing the current amplitude during the test pulse by the amplitude measured during the corresponding conditioning pulse. Fractional recovery is plotted on a log scale as a function of recovery time for (*A*) α subunits alone, (*B*) α + β_1 subunits, (*C*) α + β_2 subunits, and (*D*) α + β_1 + β_2 subunits. Data for Rat1 are indicated by *solid circles*, and data for Rat2 are indicated by *open circles*. Values represent averages, and error bars indicate SDs. The data were fit with a double or triple exponential equation as described in Materials and Methods, and the parameters of the fits are shown in Table 1. Sample sizes were Rat1 α (4), Rat2 α (5), Rat1 α + β_1 (3), Rat2 α + β_1 (4), Rat1 α + β_2 (5), Rat2 α + β_2 (3), Rat1 α + β_1 + β_2 (4), and Rat2 α + β_1 + β_2 (5).

(Fig. 4*B*). The faster recovery resulted from three effects of β_1. First, >80% of the current recovered with the fast time constant. Second, both τ_1 and τ_2 were decreased for both channels. Third, the very long time constant (τ_3) was minimal or nonexistent. Coexpression of just β_2 with the α subunits resulted in recovery kinetics that were similar to those observed for the α subunits alone, except that the fast time constant (τ_1) was decreased for both Rat1 and Rat2 (Fig. 4*C*, Table 1). When both β_1 and β_2 were coexpressed with the α subunits, recovery was similar to that observed with just α and β_1, in that most of the current recovered from inactivation with the fast time constant (Fig. 4*D*, Table 1).

The voltage dependence of activation and inactivation is more positive for Rat1 than for Rat2 sodium channels

The effects of sodium channels on electrical excitability of a neuron depend on both the kinetics and voltage dependence of sodium channel activation and inactivation. We therefore compared the voltage dependence of activation and inactivation for the Rat1 and Rat2 channels to determine whether there were any differences in these properties (Fig. 5). The curves were fit with two-state Boltzmann equations as described in Materials and Methods, and the parameters of the fits are shown in Table 1. When the α subunits were expressed alone, there were no significant differences in the voltage dependence of conductance between Rat1 (Fig. 5*A*, *filled circles*) and Rat2 (Fig. 5*A*, *open circles*). When β_1 was coexpressed with the α subunits, the conductance curves for the two channel isoforms were still similar, although the voltage for half-maximal activation ($V_{1/2}$) for Rat2 was shifted slightly in the negative direction, although not to a statistically significant extent (Fig. 5*B*, Table 1). Coexpression of the β_2 subunit with the α subunits did not significantly affect the voltage dependence of conductance compared with the α subunits alone (Fig. 5*C*, Table 1). When both β_1 and β_2 were coexpressed with the α subunits, the $V_{1/2}$ for Rat1 was shifted in the positive direction, whereas the $V_{1/2}$ for Rat2 was shifted in the negative direction, so that these two values (−15 and −22 mV) were

Table 1. Parameters of the voltage dependence of activation and inactivation and recovery from inactivation

	Activation			Inactivation			Recovery from inactivation						
							τ_1		τ_2		τ_3		
Channel	$V_{1/2}$ (mV)	z (e_o)	n	$V_{1/2}$ (mV)	a (mV)	n	msec	%	msec	%	msec	%	n
Rat1	−17 ± 4	4.8 ± 0.5	8	−35 ± 2	5.2 ± 0.5	6	1.9 ± 0.6	34 ± 4	46 ± 27	30 ± 12	280 ± 130	36 ± 13	4
Rat1 + β_1	−18 ± 1	4.2 ± 0.2*	5	−43 ± 2*	5.1 ± 0.6	6	1.1 ± 0.1	89 ± 1*	18 ± 10	7.1 ± 2.4*	ND[a]	ND[a]	3
Rat1 + β_2	−19 ± 4	5.1 ± 1.0	6	−37 ± 2	6.1 ± 0.3*	6	0.9 ± 1.1	26 ± 6	45 ± 25	46 ± 18	ND[b]	ND[b]	5
Rat1 + β_1 + β_2	−15 ± 2	3.9 ± 0.4*	6	−41 ± 2*	4.8 ± 0.6	3	1.4 ± 0.6	82 ± 1*	13 ± 4	8.6 ± 4.0*	ND[b]	ND[b]	4
Rat2	−18 ± 5	5.0 ± 1.2	10	−42 ± 4	7.4 ± 1.0	3	3.3 ± 0.6	39 ± 9	130 ± 20	44 ± 9	890 ± 360	17 ± 5	5
Rat2 + β_1	−21 ± 5	4.7 ± 0.5	7	−52 ± 1*	5.3 ± 0.6*	7	1.8 ± 0.2*	92 ± 3*	26 ± 5*	7.8 ± 3.0*	ND[c]	ND[c]	4
Rat2 + β_2	−18 ± 7	4.4 ± 0.2	5	−45 ± 2	6.8 ± 0.3	5	1.3 ± 0.9*	35 ± 5	60 ± 30*	44 ± 8	ND[b]	ND[b]	3
Rat2 + β_1 + β_2	−22 ± 4	4.5 ± 0.4	5	−57 ± 4*	4.5 ± 0.3*	5	2.2 ± 0.2*	93 ± 1*	47 ± 44*	3.5 ± 2.3*	ND[a]	ND[a]	5

*Indicates a statistically significant difference from α subunit alone at $p < 0.05$.

[a]ND, Not determined because the percentage of current recovering with τ_3 was <4%.

[b]ND, Not determined because the time constant was >1 sec and could not be accurately quantified.

[c]ND, Not determined because recovery for these channels was best fit with a double-exponential equation.

significantly different from each other (Fig. 5*D*, Table 1). The slope factors (z) were not significantly different between Rat1 and Rat2, and only the Rat1 slope factor was significantly decreased by coexpression of β_1 (Table 1). Coexpression of β_2 did not significantly change the slope factor of either Rat1 or Rat2. In summary, the voltage dependence of conductance was similar for Rat1 and Rat2 α subunits alone, but it was significantly more positive for Rat1 + β_1 + β_2 compared with Rat2 + β_1 + β_2.

With respect to the voltage dependence of inactivation, the curve for the Rat1 α subunit alone (Fig. 5*A*, *filled squares*) is shifted in the positive direction compared with that for the Rat2 α subunit alone (Fig. 5*A*, *open squares*). When β_1 was coexpressed with the α subunits, the $V_{1/2}$ values for both curves were shifted in the negative direction to a similar extent (Fig. 5*B*, Table 1). Coexpression of β_2 with the α subunits did not significantly affect the $V_{1/2}$ for either Rat1 or Rat2 compared with the α subunits alone (Fig. 5*C*, Table 1). The combination of β_1 and β_2 shifted the $V_{1/2}$ for Rat1 by −6 mV, and it shifted the $V_{1/2}$ for Rat2 by −15 mV, so that the $V_{1/2}$ for Rat2 + β_1 + β_2 was significantly more negative than that for Rat1 + β_1 + β_2 (Fig. 5*D*, Table 1). The slope factor (a) for the Rat1 α subunit was significantly smaller than that for the Rat2 α subunit alone. However, the addition of β_1 or β_1 + β_2 decreased only the Rat2 slope factor, so that it was comparable to that of Rat1 with either β_1 or β_1 + β_2. In summary, the voltage dependence of inactivation for Rat1 was significantly more positive than that for Rat2, and this effect was more pronounced when both the β_1 and β_2 subunits were present.

Rat1 sodium channel current is modulated by PKA phosphorylation

Electrical excitability of a neuron can be altered by modulating the activity of the sodium channels (Schiffmann et al., 1995). The Rat2 sodium channel is functionally modulated by PKA in Chinese hamster ovary cells (Li et al., 1992, 1993) and in *Xenopus* oocytes (Gershon et al., 1992; Smith and Goldin, 1996). Phosphorylation at PKA consensus sites in the cytoplasmic linker between domains I and II of the Rat2 channel reduces sodium current amplitude by 10–20% (Smith and Goldin, 1996, 1997). The I–II linker in Rat1 contains five consensus PKA sites at positions comparable to those in Rat2, although the amino acid sequences of the PKA sites in the two channels are not identical. It seemed likely that the Rat1 channel would also be modulated by PKA. To determine whether modulation occurred, sodium currents were measured during depolarizations to −10 mV before and 10 min after induction of PKA by perfusion with a mixture containing 25 μM forskolin, 10 μM cpt-cAMP, 10 μM db-cAMP, and 10 μl BMX. Application of the PKA-activating mixture reduced sodium current amplitude for Rat1 by 7 ± 4% (n = 8) and for Rat2 by 9 ± 5% (n = 9). Therefore, the PKA-activating mixture modulated the Rat1 sodium channel to cause a reduction in current amplitude comparable to that observed for the Rat2 channel.

DISCUSSION

We have constructed a full-length cDNA clone encoding the Rat1 sodium channel. Injection into *Xenopus* oocytes of RNA transcribed from this clone resulted in macroscopic currents that were sufficiently large for electrophysiological analysis, in contrast to the results with the original Rat1 clone (Noda et al., 1986b). The Rat1 clone that we constructed differs at four amino acid positions compared with the original Rat1 clone (Noda et al., 1986a). We do not know whether these differences represent actual polymorphisms in the rat population or are artifacts of cloning either this channel or the original Rat1 clone. Three of the differences are in cytoplasmic regions, and two of these are conservative changes. The notable exception is at position 979 in domain IIS6, where the Rat1 clone that we isolated contains a glycine and the clone isolated by Noda et al. (1986a) contains an arginine. All other voltage-gated sodium channels that have been sequenced thus far contain a glycine at the comparable position (Goldin, 1995). It is possible that this difference accounts for the fact that we observed significant sodium currents from Rat1 and Noda et al. (1986b) did not.

The level of current expressed from Rat1 in our studies was significantly less than that expressed from Rat2. A 500-fold greater amount of Rat1 RNA was injected to yield current amplitudes comparable to those observed for Rat2. This difference in current levels represents either a difference in the amount of protein (resulting from less efficient post-translational processing or insertion into the membrane or both), or it might represent a functional property of the Rat1 channel.

Rat1 sodium channels were modulated by the β_1 subunit in a manner similar to that observed previously for the Rat2 channel (Isom et al., 1992). The primary effects were a faster time course of fast inactivation, accelerated recovery from fast inactivation,

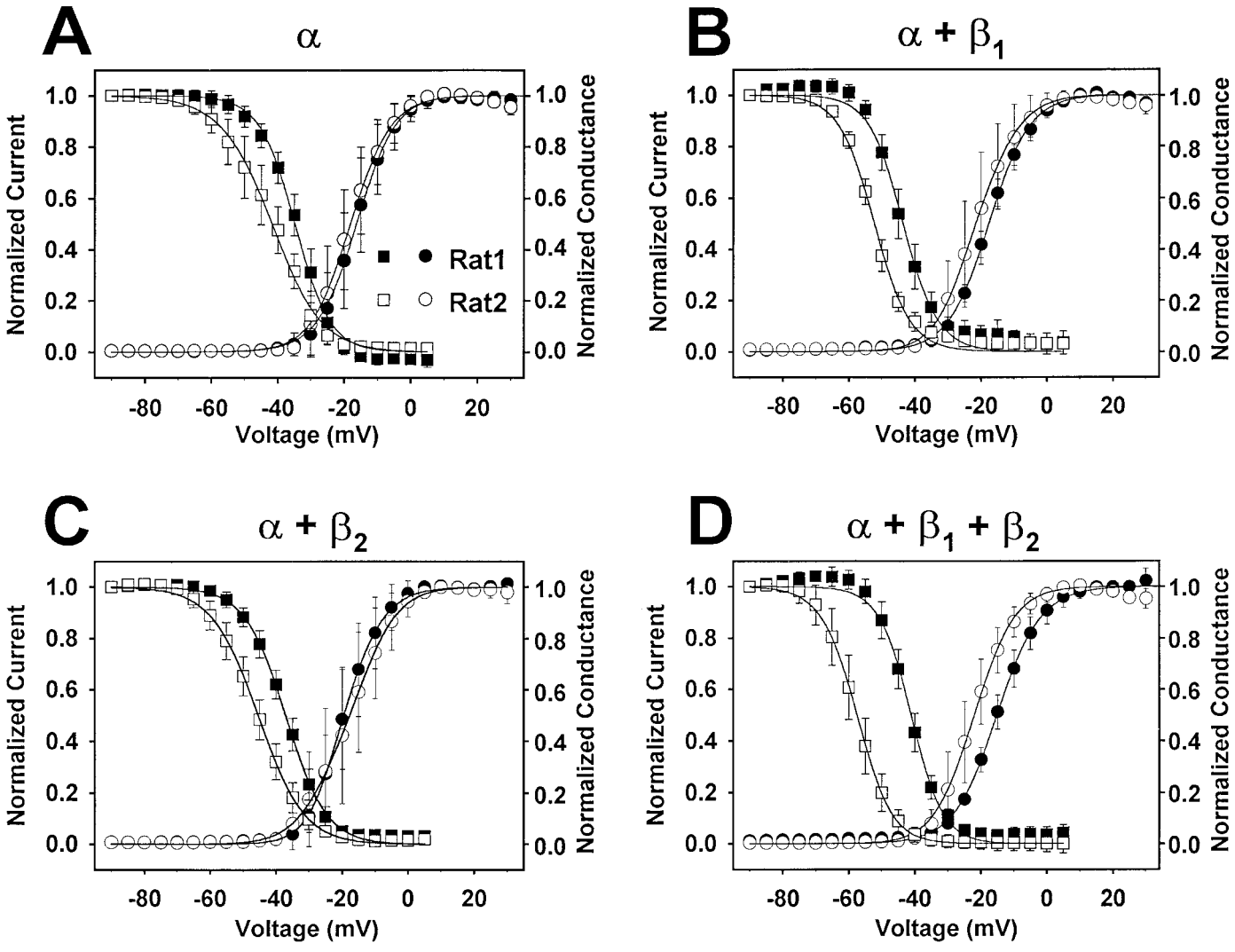

Figure 5. Voltage dependence of activation and inactivation for Rat1 and Rat2 sodium channels. The voltage-dependence of activation (*circles*) and inactivation (*squares*) are shown for (*A*) α subunits alone, (*B*) $\alpha + \beta_1$ subunits, (*C*) $\alpha + \beta_2$ subunits, and (*D*) $\alpha + \beta_1 + \beta_2$ subunits. Sodium currents were elicited by depolarizing pulses from a holding potential of −100 mV to potentials ranging from −90 to +30 mV in 5 mV increments. Conductance values were calculated by dividing the peak current amplitude by the driving force at each potential and normalizing to the maximum conductance, as described in Materials and Methods. *Solid circles* indicate Rat1, and *open circles* indicate Rat2. Values represent averages, and error bars indicate SDs. The data were fit with a two-state Boltzmann equation as described in Materials and Methods, and the parameters of the fits are shown in Table 1. Sample sizes were Rat1 α (8), Rat2 α (10), Rat1 $\alpha + \beta_1$ (5), Rat2 $\alpha + \beta_1$ (7), Rat1 $\alpha + \beta_2$ (6), Rat2 $\alpha + \beta_2$ (5), Rat1 $\alpha + \beta_1 + \beta_2$ (6), and Rat2 $\alpha + \beta_1 + \beta_2$ (5). The voltage dependence of inactivation was determined using a two-step protocol in which a conditioning pulse to potentials ranging from −90 mV to +5 mV was followed by a test pulse to −10 mV to measure the peak current amplitude. The peak current amplitude during the test pulse was normalized to the maximum current amplitude and is plotted as a function of the conditioning pulse potential. *Solid squares* indicate Rat1, and *open squares* indicate Rat2. Values represent averages, and error bars indicate SDs. The data were fit with a two-state Boltzmann equation as described in Materials and Methods, and the parameters of the fits are shown in Table 1. Sample sizes were Rat1 α (6), Rat2 α (3), Rat1 $\alpha + \beta_1$ (6), Rat2 $\alpha + \beta_1$ (7), Rat1 $\alpha + \beta_2$ (6), Rat2 $\alpha + \beta_2$ (5), Rat1 $\alpha + \beta_1 + \beta_2$ (3), and Rat2 $\alpha + \beta_1 + \beta_2$ (5).

and a negative shift in the voltage dependence of inactivation. The effect of the β_2 subunit on Rat1 was a slight acceleration of the kinetics of inactivation, similar to the effect of β_2 on the Rat2 channel (Isom et al., 1995). The combination of β_1 and β_2 with either Rat1 or Rat2 resulted in properties similar to those observed when only β_1 was coexpressed with the α subunit. It is likely that both Rat1 and Rat2 α subunits are associated with β_1 and β_2 subunits in the CNS, so that the physiologically relevant properties are those determined in the presence of all three subunits.

The kinetics of fast inactivation for the Rat1 α subunit channels were slower than those for the Rat2 α subunit channels (Figs. 2*A*, 3*A*); however, coexpression of the β_1 subunit caused the two channels to have inactivation kinetics that were comparable (Figs. 2*B*, 3*B*), so that both channels probably have similar inactivation kinetics *in vivo*. In the presence of β_1, Rat1 recovered from inactivation more quickly than Rat2, particularly at short recovery intervals of <10 msec (Fig. 4*B*). Therefore, on the basis of the kinetics of inactivation and recovery, Rat1 channels should be capable of transmitting higher frequencies of electrical impulses compared with the Rat2 channel.

The electrical excitability of sodium channels is affected by both the kinetics of inactivation and the voltage-dependent properties of the channels. When expressed in the absence of the β

subunits, the Rat1 and Rat2 channels had similar voltage dependence of conductance curves (Fig. 5*A*); however, coexpression of both β_1 and β_2 significantly shifted the $V_{1/2}$, for Rat2 in the negative direction relative to the $V_{1/2}$ for Rat1 (Fig. 5*D*, Table 1). Therefore, Rat1 channels with β_1 and β_2 would require a stronger depolarization for a comparable level of activation. With respect to the voltage dependence of inactivation, the $V_{1/2}$ for Rat1 α subunit channels was more positive than that for Rat2 α subunit channels (Fig. 5*A*). This difference was magnified by the presence of β_1 and β_2 subunits, because their presence caused a larger negative shift in the $V_{1/2}$ of Rat2 channels than for Rat1 channels (Fig. 5*D*, Table 1). The differences between Rat1 and Rat2 channels in the voltage dependence of activation and inactivation would have opposite physiological effects. The more positive $V_{1/2}$ of activation for Rat1 would mean that Rat1 channels require a stronger depolarization to be activated. In contrast, the more positive $V_{1/2}$ of inactivation would make those channels less likely to be inactivated than Rat2 channels, resulting in more channels available to be activated. Because the difference in the $V_{1/2}$ of inactivation is greater than that of activation, the net effect should be that Rat1 sodium channels are more available to transmit electrical impulses.

The excitability of sodium channels in neurons can be modulated by extrinsic factors such as phosphorylation. In particular, induction of PKA phosphorylation reduces current amplitudes through Rat2 sodium channels (Gershon et al., 1992; Li et al., 1992, 1993; Smith and Goldin, 1996), and this effect is observed in hippocampal neurons in which dopaminergic receptors are activated (Cantrell et al., 1997). In this study, the Rat1 sodium channel currents were similarly reduced by a PKA-activating mixture containing forskolin, cpt-cAMP, db-cAMP, and IBMX. We have demonstrated previously that this mixture reduces Rat2 sodium current amplitudes by induction of PKA phosphorylation of the channel, and that elimination of the consensus PKA sites in the I–II linker prevents that effect (Smith and Goldin, 1997). It is likely that the same mechanism is responsible for the reduction of Rat1 currents. Rat1 and Rat2 have the same number and positioning of the five consensus PKA sites in the cytoplasmic linker connecting domains I and II. Three of the five PKA sites have identical amino acid sequences (site 2: RRNS; site 3: RRDS; site 5: KRRSSS), and the other two sites differ by one amino acid [site 1: KR**F**SS (Rat2), KR**Y**SS (Rat1); site 4: RR**P**S (Rat2), RR**N**S (Rat1)]. The second PKA site is of critical importance in PKA-mediated current reduction for Rat2 (Smith and Goldin, 1997) and is identical in both channel isoforms.

The electrical responses of neurons in the CNS are largely determined by the properties of the channels that are expressed in those cells. Sodium channels that inactivate rapidly cause the transient, inward currents representative of fast action potentials, whereas persistent or noninactivating sodium channels may be responsible for spontaneous action potentials and plateau potentials (Llinas, 1988; Taylor, 1993; Grill, 1996). These two distinct sodium channel conductances have been well characterized in cerebellar Purkinje cells (Llinas and Sugimori, 1980; Raman and Bean, 1997). Vega-Saenz de Miera et al. (1997) suggested that the inactivating and noninactivating sodium conductances result from expression of Rat1 and Rat6, respectively. Rat2 RNA was undetectable in Purkinje cells in that study (Vega-Saenz de Miera et al., 1997). The role of Rat6 has been examined by electrophysiological analysis of Purkinje cells from ataxic mice that either lack or have a mutant form of Scn8a, the murine ortholog of Rat6 (Burgess et al., 1995; Kohrman et al., 1995; Kohrman et al., 1996). These studies indicated that Scn8a channels are responsible for subthreshold currents, suggesting that the rapidly inactivating sodium current results from Rat1 channels (Raman et al., 1997). The electrophysiological properties that we have demonstrated for Rat1 sodium channels are consistent with this conclusion.

In summary, we have constructed a full-length cDNA clone for the Rat1 sodium channel and demonstrated that this channel is functional in *Xenopus* oocytes. Some of the electrophysiological properties of Rat1 differ from those of Rat2, which would result in greater availability of Rat1 channels. These differences suggest that Rat1 channels are capable of more rapid firing of action potentials compared with Rat2 channels. In addition, the electrophysiological properties of the Rat1 channels are consistent with a role for these channels in mediating the rapidly inactivating transient current in cerebellar Purkinje cells. The availability of a functional clone for Rat1 will make it possible to evaluate the physiological role of this sodium channel isoform.

REFERENCES

Auld VJ, Goldin AL, Krafte DS, Marshall J, Dunn JM, Catterall WA, Lester HA, Davidson N, Dunn RJ (1988) A rat brain Na^+ channel α subunit with novel gating properties. Neuron 1:449–461.

Beckh S, Noda M, Lubbert H, Numa S (1989) Differential regulation of three sodium channel messenger RNAs in the rat central nervous system during development. EMBO J 8:3611–3636.

Black JA, Yokoyama S, Higashida H, Ransom BR, Waxman SG (1994) Sodium channel mRNAs I, II and III in the CNS: cell-specific expression. Mol Brain Res 22:275–289.

Burgess DL, Kohrman DC, Gait J, Plummer NW, Jones JM, Spear B, Meisler MH (1995) Mutation of a new sodium channel gene, *Scn8a*, in the mouse mutant "motor endplate disease." Nature Genet 461–465.

Cantrell AR, Smith RD, Goldin AL, Scheuer T, Catterall WA (1997) Dopaminergic modulation of sodium current in hippocampal neurons via cAMP-dependent phosphorylation of specific site(s) in the sodium channel α subunit. J Neurosci 17:7330–7338.

Crill WE (1996) Persistent sodium current in mammalian central neurons. Annu Rev Physiol 58:349–362.

Dierks P, van Ooyen A, Mantel N, Weissmann C (1981) DNA sequences preceding the rabbit β-globin gene are required for formation in mouse L cells of beta-globin RNA with the correct 5′ terminus. Proc Natl Acad Sci USA 78:1411–1415.

Felts PA, Yokoyama S, Dib-Hajj S, Black JA, Waxman SG (1997) Sodium channel α-subunit mRNAs I, II, III, NaG, Na6 and hNE (PN1): different expression patterns in developing rat nervous system. Mol Brain Res 45:71–82.

Furuyama T, Morita Y, Inagaki S, Takagi H (1993) Distribution of I, II and III subtypes of voltage-sensitive Na^+ channel mRNA in the rat brain. Mol Brain Res 17:169–173.

Gautron S, Dos Santos G, Pinto-Henrique D, Koulakoff A, Gros F, Berwald-Netter Y (1992) The glial voltage-gated sodium channel: cell- and tissue-specific mRNA expression. Proc Natl Acad Sci USA 89:7272–7276.

Gershon E, Weigl L, Lotan I, Schreibmayer W, Dascal N (1992) Protein kinase A reduces voltage-dependent Na^+ current in *Xenopus* oocytes. J Neurosci 12:3743–3752.

Goldin AL (1991) Expression of ion channels by injection of mRNA into *Xenopus* oocytes. Methods Cell Biol 36:487–509.

Goldin AL (1995) Voltage-gated sodium channels. In: Ligand- and voltage-gated ion channels (North RA, ed), pp 73–112. Boca Raton, FL: CRC.

Gordon D, Merrick D, Auld V, Dunn R, Goldin AL, Davidson N, Catterall WA (1987) Tissue-specific expression of the R_I and R_{II} sodium channel subtypes. Proc Natl Acad Sci USA 84:8682–8686.

Hartshorne RP, Catterall WA (1984) The sodium channel from rat brain: purification and subunit composition. J Biol Chem 259:1667–1675.

Isom LL, DeJongh KS, Patton DE, Reber BFX, Offord J, Charbonneau H, Walsh K, Goldin AL, Catterall WA (1992) Primary structure and functional expression of the β_1 subunit of the rat brain sodium channel. Science 256:839–842.

Isom LL, Ragsdale DS, De Jongh KS, Westenbroek RE, Reber BFX,

Scheuer T, Catterall WA (1995) Structure and function of the β_2 subunit of brain sodium channels, a transmembrane glycoprotein with a CAM motif. Cell 83:433–442.

Joho RH, Moorman JR, VanDongen AMJ, Kirsch GE, Silberberg H, Schuster G, Brown AM (1990) Toxin and kinetic profile of rat brain type III sodium channel expressed in *Xenopus* oocytes. Mol Brain Res 7:105–113.

Kayano T, Noda M, Flockerzi V, Takahashi H, Numa S (1988) Primary structure of rat brain sodium channel III deduced from the cDNA sequence. FEBS Lett 228:187–194.

Kohrman DC, Plummer NW, Schuster T, Jones JM, Jang W, Burgess DL, Galt J, Spear BT, Meisler MH (1995) Insertional mutation of the motor endplate disease (*med*) locus on mouse chromosome 15. Genomics 26:171–177.

Kohrman DC, Smith MR, Goldin AL, Harris J, Meisler MH (1996) A missense mutation in the sodium channel Scn8a is responsible for cerebellar ataxia in the mouse mutant *jolting*. J Neurosci 16:5993–5999.

Kontis KJ, Rounaghi A, Goldin AL (1997) Sodium channel activation gating is affected by substitutions of voltage sensor positive charges in all four domains. J Gen Physiol 110:391–401.

Li M, West JW, Lai Y, Scheuer T, Catterall WA (1992) Functional modulation of brain sodium channels by cAMP-dependent phosphorylation. Neuron 8:1151–1159.

Li M, West JW, Numann R, Murphy BJ, Scheuer T, Catterall WA (1993) Convergent regulation of sodium channels by protein kinase C and cAMP-dependent protein kinase. Science 261:1439–1442.

Llinas RR (1988) The intrinsic electrophysiological properties of mammalian neurons: insights into central nervous system function. Science 242:1654–1664.

Llinas R, Sugimori M (1980) Electrophysiological properties of *in vitro* Purkinje cell somata in mammalian cerebellar slices. J Physiol (Lond) 305:171–195.

Noda M, Ikeda T, Kayano T, Suzuki H, Takeshima H, Kurasaki M, Takahashi H, Numa S (1986a) Existence of distinct sodium channel messenger RNAs in rat brain. Nature 320:188–192.

Noda M, Ikeda T, Suzuki H, Takeshima H, Takahashi T, Kuno M, Numa S (1986b) Expression of functional sodium channels from cloned cDNA. Nature 322:826–828.

Patton DE, Goldin AL (1991) A voltage-dependent gating transition induces use-dependent block by tetrodotoxin of rat IIA sodium channels expressed in *Xenopus* oocytes. Neuron 7:637–647.

Patton DE, Isom LL, Catterall WA, Goldin AL (1994) The adult rat brain β_1 subunit modifies activation and inactivation gating of multiple sodium channel α subunits. J Biol Chem 269:17649–17655.

Raman IM, Bean BP (1997) Resurgent sodium current and action potential formation in dissociated cerebellar Purkinje neurons. J Neurosci 17:4517–4526.

Raman IM, Sprunger LK, Meisler MH, Bean BP (1997) Altered subthreshold sodium currents and disrupted firing patterns in Purkinje neurons of Scn8a mutant mice. Neuron 19:881–891.

Schaller KL, Krzemien DM, Yarowsky PJ, Krueger BK, Caldwell JH (1995) A novel, abundant sodium channel expressed in neurons and glia. J Neurosci 15:3231–3242.

Schiffmann SN, Lledo P-M, Vincent J-V (1995) Dopamine D_1 receptor modulates the voltage-gated sodium current in rat striatal neurones through a protein kinase A. J Physiol (Lond) 483:95–107.

Smith RD, Goldin AL (1996) Phosphorylation of brain sodium channels in the I–II linker modulates channel function in *Xenopus* oocytes. J Neurosci 16:1965–1974.

Smith RD, Goldin AL (1997) Phosphorylation at a single site in the rat brain sodium channel is necessary and sufficient for current reduction by PKA. J Neurosci 17:6086–6093.

Taglialatela M, Toro L, Stefani E (1992) Novel voltage clamp to record small, fast currents from ion channels expressed in *Xenopus* oocytes. Biophys J 61:78–82.

Taylor CP (1993) Na^+ currents that fail to inactivate. Trends Neurosci 16:455–460.

Vega-Saenz de Miera E, Rudy B, Sugimori M, Llinas R (1997) Molecular characterization of the sodium channel subunits expressed in mammalian cerebellar Purkinje cells. Proc Natl Acad Sci USA 94:7059–7064.

Westenbroek RE, Merrick DK, Catterall WA (1989) Differential subcellular localization of the R_I and R_{II} Na^+ channel subtypes in central neurons. Neuron 3:695–704.